# Effects of the 2006 El Niño on tropospheric ozone and carbon monoxide: Implications for dynamics and biomass burning

S. Chandra[1,2], J. R. Ziemke[1,2], B. N. Duncan[1,2], and T. L. Diehl[1,2]

[1]Goddard Earth Sciences and Technology Center, University of Maryland Baltimore County, Baltimore, Maryland, USA

[2]NASA Goddard Space Flight Center, Greenbelt, Maryland, USA

We have studied the effects of the 2006 El Niño on tropospheric $O_3$ and CO at tropical and sub-tropical latitudes measured from the OMI and MLS instruments on the Aura satellite. The 2006 El Niño-induced drought allowed forest fires set to clear land to burn out of control during October and November in the Indonesian region. The effects of these fires are clearly seen in the enhancement of CO concentration measured from the MLS instrument. We have used a global model of atmospheric chemistry and transport (GMI CTM) to quantify the relative importance of biomass burning and large scale transport in producing observed changes in tropospheric $O_3$ and CO. The model results show that during October and November both biomass burning and meteorological changes contributed almost equally to the observed increase in tropospheric $O_3$ in the Indonesian region. The biomass component was 4-6 DU but it was limited to the Indonesian region where the fires were most intense. The dynamical component was 4-8 DU but it covered a much larger area in the Indian Ocean extending from South East Asia in the north to western Australia in the south. By December 2006, the effect of biomass burning was reduced to zero and the observed changes in tropospheric $O_3$ were mostly due to dynamical effects. The model results show an increase of 2-3% in the global burden of tropospheric ozone. In comparison, the global burden of CO increased by 8-12%.

## 1 Introduction

El Niño and La Niña events are major sources of inter-annual and decadal variability in tropical tropospheric ozone ($O_3$) [e.g., *Ziemke et al.* 2003]. The atmospheric effects of El Niño events are generally a change in convection in the tropical troposphere associated with an eastward shift of the warm SST anomaly and large scale Walker circulation. This shift results in an increase in tropospheric column $O_3$ in the western Pacific and a decrease in the eastern Pacific relative to non-El Niño years. The effect of El Niño on specific humidity is usually opposite to that of column ozone [e.g., *Chandra et al.*, 1998; 2007]. During La Niña years, dynamical processes are largely reversed which results in a decrease (increase) of column ozone (specific humidity) in the western Pacific. The effects of El Niño on tropospheric composition have been extensively studied from both satellite and ground based measurements [e.g., *Chandra et al.*, 1998; *Fujiwara et al.*, 1999; *Thompson et al.*, 2001] and by using global models of atmospheric chemistry and transport [e.g., *Peters et al.*, 2001; *Sudo and Takahashi*, 2001; *Chandra et al.*, 2002, 2003; *Duncan et al.*, 2003; *Zeng and Pyle,* 2005; *Doherty et al.*, 2006]

Recently *Logan et al.* [2008] studied the effects of the 2004 and 2006 El Niño events on tropospheric profiles of CO, $O_3$, and $H_2O$ measured from the Tropospheric Emission Spectrometer (TES) on the Aura satellite. Their findings were generally consistent with the observed characteristics of $O_3$ and $H_2O$ inferred from previous El Niño events. The changes during the 2004 El Niño in tropospheric $O_3$ and $H_2O$ from TES are similar to those inferred from Ozone Monitoring Instrument (OMI) and Microwave Limb Spectrometer (MLS) flown on the same satellite [*Chandra et al.*, 2007]. The 2004 El Niño was a weak event compared to 2006 and significantly weaker compared to the El Niño of 1997-1998. This was reflected in the TCO (tropospheric column ozone) anomaly over the Indonesian region in the western Pacific as shown in Table 1 of *Logan et al.* [2008]. For example, the TCO anomaly in November 1997 inferred from EP TOMS was 14.4 Dobson Units (DU; 1 DU = $2.69 \times 10^{20}$ molecules-m$^{-2}$). The corresponding values from TES for November 2004 and 2006 were 6.6 DU and 11.1 DU. *Logan et al.* [2008] attributed most of these changes to differences in the magnitude of CO emissions from fires in Indonesia which in these years were estimated to be 193 Tg, 24 Tg, and 82 Tg, respectively. They also suggested significant contribution from $NO_X$ production due to lightning in late November and December 2006 when CO production due to large scale forest fires

decreased significantly. The effects of forest fires in the Indonesian region during the 1997 El Niño was studied by *Chandra et al.* [2002] using the GEOS-CHEM global model of chemistry and transport. Their study suggested that about half of the increase in tropospheric column ozone in the Indonesian region was due to biomass burning and the other half due to dynamical effects. A similar conclusion was arrived by *Sudo and Takahashi* [2001] from their model study. Their conclusion about the contribution of biomass burning was indirect since they did not explicitly include the effect of biomass burning in their model study.

The combined OMI and MLS instruments on the Aura satellite have been providing near global measurements of TCO from August 2004 to present [e.g., *Ziemke et al.*, 2006; *Schoeberl et al.*, 2007] as discussed in Section 2. In addition the MLS instrument has been providing daily measurements of CO at several pressure levels in the troposphere and stratosphere [*Livesey et al.*, 2008]. The purpose of this paper is to study the effects of the 2006 El Niño on tropospheric composition measured from the OMI and MLS instruments on the Aura satellite and evaluate specific roles of the various processes using a global model of chemistry and transport. The global model used in this study is the NASA GMI CTM (Global Modeling Initiative Chemical Transport Model). It successfully simulates a wide range of observations of chemical constituents in the troposphere and stratosphere, including data collected by instruments on board satellites. We provide a brief overview of the relevant tropospheric processes in the GMI CTM in section 3. In our study, the El Niño related changes in $O_3$ and CO fields based on OMI and MLS measurements are compared with corresponding changes based on GMI CTM simulation to delineate the relative importance of biomass burning and large scale transport.

In the following, section 2 discusses the satellite data, section 3 the GMI model, and sections 4 and 5 compare observed and measured $O_3$ and CO, respectively. Section 6 discusses the impact of biomass burning emissions over Indonesia during the 2006 El Niño, and section 7 compares the strength and frequency of the 2006 and recent El Niño events with previous El Niño events. Finally, section 8 provides a summary.

## 2 Measurements from OMI and MLS

OMI is one out of a total of four instruments onboard the Aura spacecraft which is flown in a sun-synchronous polar orbit at 705 km altitude with a 98.2° inclination. The spacecraft has an equatorial crossing time of 1:45 pm (ascending node) with around 98.8 minutes per orbit (14.6 orbits per day on average). OMI is a nadir-scanning instrument that for visible (350-500 nm) and UV wavelength channels (UV-1: 270-314 nm; UV-2: 306-380 nm) detects backscattered solar radiance to measure column ozone with near global coverage (aside from polar night latitudes) over the Earth with a resolution of 13 km × 24 km at nadir. Besides ozone OMI also measures cloud-top pressure, aerosols and aerosol parameters, $NO_2$, $SO_2$, and other trace constituents in the troposphere and stratosphere [*Levelt et al.*, 2006]. Total ozone from OMI is derived from the TOMS version 8 algorithm. A description of this algorithm may be obtained from the TOMS V8 CD DVD ROM, or from the OMI Algorithm Theoretical Basis Document (ATBD) (from the webpage http://toms.gsfc.nasa.gov/version8/v8toms_atbd.pdf).

There are two standard OMI total ozone products. Here we use data from the collection 3 OMTO3 version 8.5 (v8.5) product that is based on the Total Ozone Mapping Spectrometer (TOMS) version 8 (v8) total $O_3$ algorithm. A description of this algorithm may be obtained from the TOMS v8 DVD or the OMI Algorithm Theoretical Basis Document (ATBD) from the TOMS web page http://toms.gsfc.nasa.gov/version8/v8toms_atbd.pdf. A main difference between v8 and v8.5 is that v8.5 uses measured cloud pressure whereas v8 and earlier versions used an infrared-measured climatology for cloud pressure. Another OMI algorithm based on the Differential Optical Absorption Spectroscopy Method (DOAS) technique gives similar estimates of total column ozone [*Kroon et al.*, 2008b]. These total column $O_3$ retrievals have been compared with ground-based data [*McPeters et al.*, 2008] and aircraft-based measurements [*Kroon et al.*, 2008a].

$O_3$ profiles from the Aura Microwave Limb Sounder (MLS) are used to estimate stratospheric column $O_3$ (SCO). The SCO is subtracted from OMI total column $O_3$ from OMI to yield tropospheric column $O_3$ and mean volume mixing ratio [e.g., *Ziemke et al.*, 2006]. The mean volume mixing ratio (units ppbv) is determined by taking tropospheric column $O_3$ (in Dobson Units, DU) and dividing this by pressure difference (in units hPa) between surface and tropopause, and then multiplying this by the factor 1.27. Validation of MLS v2.2 measurements is discussed by *Froidevaux et al.* [2008] and *Livesey et al.* [2008]. The measurements of mean

tropospheric $O_3$ from OMI/MLS and upper tropospheric CO from MLS are studied and compared with simulations from a global chemical transport model (discussed next).

## 3 NASA Global Modeling Initiative Chemical Transport Model

The GMI CTM is described and evaluated in *Ziemke et al.* [2006], *Schoeberl et al.* [2006], *Strahan et al.* [2007] and *Duncan et al.* [2007, 2008]. The chemical mechanism includes 117 species, 322 chemical reactions, and 81 photolysis reactions to simulate tropospheric and stratospheric chemistry. It includes a detailed description of $O_3$-$NO_X$-hydrocarbon chemistry, updated with recent experimental data. The chemical mass balance equations are integrated using the SMVGEAR II algorithm [*Jacobson*, 1995]. Photolysis frequencies are computed using the Fast-JX radiative transfer algorithm (M. Prather, *personal communication*). The algorithm treats both Rayleigh scattering as well as Mie scattering by clouds and aerosol. The CTM simulates the radiative and heterogeneous chemical effects of sulfate, dust, sea-salt, organic carbon and black carbon aerosol on tropospheric photochemistry.

Biogenic emissions of isoprene and monoterpenes are calculated on-line as described in *Guenther et al.* [2006]. The lightning $NO_X$ parameterization fits the relationship between model-calculated convective mass fluxes and observed cloud-to-ground flash rates (D. Allen and K. Pickering, *personal communication*). Time-appropriate anthropogenic and biomass burning emissions include, surface emissions from industry/fossil fuel, biomass burning, biogenic and biofuel combustions and contributions from aircraft emissions. They are based on the Global Fire Emission Database, version 2 (GFEDv2) and discussed in the GMI CTM papers listed above. Monthly total biomass burning of CO and $NO_X$ are shown in Table 1 for the later part of 2006 when the Indonesian fires were most intense.

Table 1 indicates that the Indonesian fires increased the CO burden by 69 Tg during the three month period from September to November 2006. It is about 27% of the global CO burden (251 Tg) during the same period. The increase in $NO_X$ due to Indonesian fires during the same period was 1.19 Tg compared to the global burden of about 19.4 Tg.

The meteorological fields that drive transport are from the Goddard Modeling and Assimilation Office (GMAO) GEOS-4 data assimilation system (GEOS-4-DAS) [*Bloom et al.*, 2005]. Features of the circulation, such as anticyclones, in the GMI CTM are realistically represented in

the simulations because of the data constraints on meteorological analyses. The GEOS-4-DAS fields have been regridded to 42 vertical levels with a lid at 0.01 hPa. The horizontal resolution is 2.5° × 2° (longitude by latitude).

A validation of the global model used in this study is given in the Appendix. This analysis compares the zonal and seasonal variability of TCO derived from the model with observed variability from OMI/MLS.

## 4 Model comparison of El Niño related changes in $O_3$ with satellite measurements

As in *Chandra et al.* [2007] and *Logan et al.* [2008], we have chosen October, November and December 2005 as a baseline for estimating El Niño-related changes in these months in the preceding and the following year. Year 2005 was a neutral year from an El Niño perspective. Maps of tropospheric $O_3$ mean mixing ratio are shown in Figure 1a for October 2004, 2005, and 2006. They show relative changes in ozone in the El Niño years (upper and lower panels) with respect to a non El Niño year (middle panel). All three panels show regions of minimum values near the dateline. However, both the upper and the lower panels show a greater eastward shift across the dateline which results in an increase of about 6-15 ppbv (~4-10 DU) over the western Pacific region and a decrease of smaller magnitude east of the dateline. The increase in $O_3$ mean mixing ratio is larger in October 2006 (lower panel) which is consistent with a relatively stronger El Niño event in 2006 compared to 2004. The model (Figure 1b) captures most of the zonal characteristics of TCO shown in Figure 1a, but it tends to underestimate the observed values by 5-10 ppbv over most of the region between ±10 deg. (Figure 1c). Outside this region the sign is reversed and the model is biased higher by about the same magnitude. These pattern shifts in the model and observation are comparable in November and December months (not shown) and are similar to those shown in Figure 2 of *Ziemke et al* [2000] for the 1997 El Niño event.

The El Niño related changes in ozone mean mixing ratio in 2006 are clearly discernible in Figures 2a, 2b and 2c. These figures show differences in OMI/MLS $O_3$ (top panels) and the model $O_3$ (bottom panels) between years 2006 and 2005 for the months of October-December. The model and observed values are generally in good agreement except in the western Pacific region in October (Figure 2a) where the model values are biased higher. This bias is also reflected in CO as indicated in section 5 and is probably due to overestimation of the effect of

biomass burning in the Indonesian region in October 2006. In general, observations and model indicate excellent agreement in characterizing both broad and small scale features including the dipole nature of ozone anomaly in the tropical Pacific region (Figures 2a and 2c). The large negative anomaly over eastern Africa/Indian Ocean in December 2006 seen in the data (Figure 2c) is a manifestation of dynamically induced changes and is well produced in the model. We have analyzed the model results to estimate the contributions of the upper (above 500 hPa) and the lower troposphere in producing the El Niño related changes in tropospheric ozone. In general, the contributions from the upper and the lower troposphere are almost equal. However, the large negative anomaly in December in the eastern Africa/Indian Ocean (Figure 2c) comes mostly from the upper troposphere.

## 5 Model Comparison of CO with satellite measurements

The El Niño events of 2004 and 2006 caused droughts in the Indonesian region which allowed set fires to spread uncontrolled in both October and November of these years. The MLS measurements show a relatively larger increase in CO in 2006 as compared to 2004 (figure not shown). This is consistent with CO measurements from TES [*Logan et al.*, 2008]. The model results show CO to be well mixed in the free troposphere even though convection was greatly reduced in this region. During October 2006, the model shows an increase of about 200 ppbv in the Indonesian region over much of the free troposphere. Figures 3a-3c show differences in upper tropospheric CO from MLS (top panels) and the model (bottom panels) between 2006 and 2005 for October-December. In October, both the model and measurements show elevated values of CO in 2006 over the Indonesian region in the western Pacific. One month later in November (Figure 3b) upper tropospheric CO from both MLS and the model are greatly reduced. They become negligible by December as the fire subsides in this region. CO for both measurement and model exhibit very similar spatial and temporal patterns except in October 2006 (Figure 3a). The model shows a sharp horizontal gradient with CO mixing ratio exceeding 200 ppbv in the Indonesian region. The MLS values of CO and horizontal gradients are significantly smaller, largely due to the coarser spatial resolution of MLS nadir measurements which were interpolated horizontally between orbital tracks. It is interesting to note that the large increase in CO in 2006 during October-November nearly disappears in December, yet $O_3$

in December in the western Pacific remains elevated (Figure 2c). *Logan et al.* [2008] attribute some of these increases in $O_3$ due to lightning $NO_X$ in the Indonesian region.

## 6 Impact of biomass burning during the 2006 El Niño

In sections 4 and 5 we analyzed the El Niño related changes in tropospheric $O_3$ and CO in 2006 using both the model and observations. In this section we analyze the model results to estimate the relative importance of biomass burning and large scale transport in producing the El Niño related changes in tropospheric $O_3$. Our approach is similar to the one used by *Chandra et al.* [2002] in analyzing the effect of the 1997 El Niño on tropospheric $O_3$. The model was run in two modes: The first mode explicitly included the $NO_X$ and CO emission rates associated with the Indonesian fires as given in Table 1. The results of these runs are discussed in sections 4 and 5. In the second mode, the model was run by excluding the contributions from the Indonesian fires. The model runs in this mode are used to assess the effects of large scale transport on tropospheric $O_3$ as shown in the bottom panels of Figures 4a-4c. The difference of the two runs gives the contribution from biomass burning as shown in the upper panels of Figures 4a-4c.

In October 2006 the increase in $O_3$ due to biomass burning is about 4-6 DU (Figure 4a, upper panel). This increase is limited to a small region comprising the islands of Sumatra, Java and Borneo in the Indonesian region. It is comparable to 4-8 DU increase caused by changes in meteorological conditions (Figure 4b, lower panel). The latter, however, extends over a much larger area in the Indian Ocean encompassing regions of the Indian subcontinent and south-east Asia in the north, to western Australia in the south. These patterns are essentially similar in November 2006 (Figure 4b). In December, 2006, the $O_3$ increase due to biomass burning is reduced to zero and the dynamical component of the $O_3$ field is identical to Figure 2c (lower panel).

Table 2 shows the model simulations of monthly averaged global tropospheric burden of CO, $O_3$ and $NO_X$ with and without Indonesian fire emissions. The table shows that during October 2006 the Indonesian fires contributed about 36 Tg which was about 10.7% of the global budget of CO. The increase in CO during November and December were respectively 12.6% and 8.1% of the global budget. These changes are significant and suggest that the El Niño related fires in the Indonesian region may have contributed significantly to global pollution. In comparison the

impact of fire was relatively small (< 3%) on the global $O_3$ burden. *Logan et al.* [2008] have suggested $NO_X$ production due to lightning as a contributing factor to the positive anomaly in TCO during December 2006. The $NO_X$ production due to lightning is implicitly included in the model calculations. In the tropical Pacific region (12°S-12°N, 90°E-170°E), lightning produced a total of 0.032 Tg NO in October 2006. This value increased to 0.0492 Tg NO in November and 0.0562 Tg NO in December 2006.

## 7 The El Niño of 2006: A long-term perspective

Though the main focus of this study is the El Niño event of 2006, such events are very frequent and may have significant impact on global pollution. According to the World Meteorological Organization (WMO) an El Niño (La Niña) event is identified when sea surface temperature (SST) in the Niño 3.4 region (5°S-5°N, 120°W-170°W) is at least 0.5°C above (below) normal when averaged over three consecutive months. The relation between ΔSST and ΔTCO (the difference in TCO between eastern and western Pacific) is shown in Figure 5. The ΔTCO time series is derived by subtracting TCO in the eastern Pacific (15°S-15°N, 135°W-180°) from TCO in the western Pacific (15°S-15°N, 95°E-140°E). The time series is deseasonalized and smoothed with a three-month running average to be compatible with Niño 3.4 SST. TCO is derived from 29 years (1979-2008) of total column ozone measurements from Nimbus 7 TOMS, Earth Probe TOMS and OMI using the convective cloud differential (CCD) method [e.g., *Ziemke et al.*, 2005]. Figure 5 shows a very robust correlation between ΔSST and ΔTCO. Even though the 1997 El Niño produced largest perturbations in SST and TCO in the tropical Pacific, El Niño events like 2006 are more common. They are also episodic. Before 1997 they occurred about every 3-4 years, but more recently they have occurred every 2 years. A frequent occurrence of El Niño, similar to 2006, has the potential of increasing the global pollution triggered by the dryness and the resulting forest fires in the Indonesian region.

## 8 Summary and Conclusion

We have studied the effects of the 2006 El Niño on tropospheric $O_3$, and CO at tropical and sub-tropical latitudes measured from the OMI and MLS instruments on the Aura satellite. The zonal characteristics of observed changes in these constituents are similar to those reported by *Logan et al.* [2008] based on measurements of these constituents from the TES instrument on the same

satellite. During October and December 2006, both these studies revealed a dipole like structure in TCO in the tropics with an increase over the western Pacific region and a decrease over the eastern Pacific region. The dipole structure was weaker during November 2006.

The 2006 El Niño-induced drought allowed forest fires to spread rapidly during October and November in the Indonesian region. The effects of these fires are clearly seen in the enhancement of CO concentration measured from both the MLS and TES instruments. We have used a global model of atmospheric chemistry and transport (GMI CTM) to quantify the relative importance of biomass burning and large scale transport in producing observed changes in TCO. The model results show that during October and November both biomass burning and meteorological changes contributed almost equally to increases in TCO in the Indonesian region. The biomass component was 4-6 DU but it was limited to the Indonesian region where the fires were most intense. The dynamical component was 4-8 DU but it covered a much larger area in the western Pacific and Indian Ocean extending from South East Asia in the north to western Australia in the south. During December 2006 the effect of biomass burning was reduced to zero and the observed changes in TCO were mostly due to dynamical effects. *Chandra et al.* [2002] have obtained similar results for the 1997 El Niño using ozone measurements from Earth Probe TOMS and comparing them with the GEOS-CHEM model. The 1997 El Niño was significantly stronger than the 2006 El Niño and caused greater perturbations in TCO due to both forest fires and large scale transport. For the 2006 El Niño the model shows an increase of 2-3% in the global burden of tropospheric ozone. In comparison, the global burden of CO increased by 8-12%.

This study shows that the 2006 El Niño can be characterized from long records of tropospheric $O_3$ and sea surface temperature as a moderate event, yet still the contribution to pollution from biomass burning emissions over Indonesia was substantial, both locally and also when evaluated on a global basis. In recent years El Niño events have occurred with greater frequency than in previous years dating back to 1979. Both the frequency and scale of emissions from biomass burning suggests that even relatively moderate El Niño events can be an important source of pollution in the troposphere.

**Acknowledgments.** The authors thank the Aura OMI and MLS instrument and algorithm teams for the extensive satellite measurements used in this study. The OMI instrument was built by

Dutch-Finnish collaboration, and is managed by the Royal Netherlands Meteorological Institute (KNMI). The authors also thank the GMI processing group for their extensive efforts in producing the GMI CTM. Data used in this study were processed at NASA Goddard Space Flight Center. Funding for this research was provided in part by Goddard Earth Science Technology (GEST) grant NGC5-494.

**Appendix: Comparisons between OMI/MLS and model $O_3$**

*Ziemke et al.* [2006] compared tropospheric ozone variability derived from OMI/MLS and the GMI CTM using earlier versions of both the model and measurements. As discussed in section 2, the total ozone data used in this paper is based on the TOMS version 8.5 algorithm instead of version 8 as used by *Ziemke et al.* [2006]. The model also uses different emission sources and meteorological fields. In the following we compare the temporal/seasonal and zonal variability of TCO fields derived from the model and the measurements under varying conditions.

Figure A1 compares the temporal and seasonal variations of the model and observations for three separate regions: American (left four panels), African (middle four panels), and Indonesian (right four panels). In each region latitudes extend from north to south with the top panel being northernmost. In northern latitudes tropospheric $O_3$ for the model and measurement maximizes around March-July. In southern latitudes largest amounts occur in September-November. In between at low latitudes the seasonal variability is small in comparison. In general the temporal variability in model and measurements are remarkably similar indicating the ability of the model to capture month-by-month variability in the data. All three top panels in Figure A1 for the latitude band 30°N-35°N show offset differences of 5-10 DU (with GMI larger than OMI/MLS). For the upper right panel in Figure A1 (corresponding to east China) the model and measured $O_3$ in summer are comparable but the model values are larger than measured values by 5-10 DU in winter and spring months when STE is greatest.

*Martin et al.* [2002] and *Chandra et. al.* [2002] compared the seasonal variability in tropospheric $O_3$ from the GEOS-Chem model and TOMS CCD measurements. A large discrepancy was found between the model and the CCD measurements over low latitudes in northern Africa including Abidjan (5°N, 4°W). The model indicated maximum tropospheric column $O_3$ around December-February during peak time of the biomass burning whereas TOMS showed greatest

amounts around June-October at a time when there is little or no biomass burning in northern Africa. Our analysis shows that the OMI measurements agree much better with model than the TOMS measurements pertaining to this seasonal variability over Africa. The GMI model indicates that enhancements in tropospheric $O_3$ over northern Africa from the biomass burning lie almost entirely below 500 hPa and are highly localized to the relatively small region of burning emissions.

Figure A2 shows statistical comparisons of model and observations. The three panels in this figure show their zonal correlations (top panel), mean zonal offset difference (middle panel) and mean zonal RMS (lower panel). The grey shading in the top panel represents areas that are not statistically significant at 99.9% confidence level. Figure A2 shows that the positive correlation between the model and OMI/MLS TCO, extending out to mid-latitudes, drops to negative values in higher latitudes. Several factors could contribute to near-zero or negative cross-correlations. Aside from known model uncertainties which include STE, OMI retrievals become less sensitive in measuring tropospheric $O_3$ in high latitudes (i.e., high solar zenith angles) and have reduced sensitivity in measuring $O_3$ in the lower troposphere, especially for high solar zenith angles and large slant columns. The model and observations compare the best in the tropics and subtropics extending out to latitudes of about $\pm 30^{\circ}$ to $\pm 35^{\circ}$. This is the latitude range chosen for GMI and OMI/MLS measurements for studying the 2006 El Niño event.

**References**

Bloom, S., et al., Documentation and validation of the Goddard Earth Observing System (GEOS) Data Assimilation System – Version 4, *Technical Report Series on Global Modeling and Data Assimilation 104606,* 2005.

Chandra, S., J. R. Ziemke, W. Min, and W. G. Read, Effects of 1997-1998 El Niño on tropospheric ozone and water vapor, *Geophys. Res. Lett., 25*, 3867-3870, 1998.

Chandra, S., J. R. Ziemke, Tropical tropospheric ozone: Implications for dynamics and biomass burning, *J. Geophys. Res., 107*(D14), doi:10.1029/2001JD000447, 2002.

Chandra, S., J. R. Ziemke, and R. V. Martin, Tropospheric ozone at tropical and middle latitudes derived from TOMS/MLS residual: Comparison with a global model, *J. Geophys. Res., 108*(D9), 4291, doi:10.1029/2002JD002912, 2003.

Chandra, S., J. R. Ziemke, M. R. Schoeberl, et al., Effects of the 2004 El Niño on tropospheric ozone and water vapor, *Geophys. Res. Lett., 34*, L06802, doi:10.1029/2006GL028779, 2007.

Doherty, R. M., D. S. Stevenson, C. E. Johnson, et al., Tropospheric ozone and El Niño-Southern Oscillation: Influence of atmospheric dynamics, biomass burning emissions, and future climate change, *J. Geophys. Res., 111*, D19304, doi:10.1029/2005JD006849, 2006.

Duncan, B. N., R. V. Martin, A. Staudt, et al., Inter-annual and seasonal variability of biomass burning emissions constrained by satellite observations, *J. Geophys. Res.*, 108, doi:10.1029/2002JD002378, 2003.

Duncan, B., et al., Model Study of the Cross-Tropopause Transport of Biomass Burning Pollution, *Atmos. Chem. Phys., 7*, 3713-3736, 2007.

Duncan, B., et al., The influence of European pollution on ozone in the Near East and northern Africa, *Atmos. Chem. Phys., 8*, 2267-2283, 2008.

Froidevaux, L., Y. B. Jiang, A. Lambert, et al., Validation of Aura Microwave Limb Sounder stratospheric ozone measurements, *J. Geophys. Res., 113*(D15), D15S20, 2008.

Fujiwara, M., K. Kita, S. Kawakami, et al., Tropospheric ozone enhancements during the Indonesian forest fire events in 1994 and in 1997 as revealed by ground-based observations, *Geophys. Res. Lett., 26*, 2417-2420, 1999.

Guenther, A., T. Karl, P. Harley, et al., Estimates of global terrestrial isoprene emissions using MEGAN (Model of Emissions of Gases and Aerosols from Nature), *Atmos. Chem. Phys., 6*, 3181-3210, 2006.

Jacobson, M., Computaton of global photochemistry with SMVGEAR II, *Atmos. Environ., 29*, 3541-2546, 1995.

Kroon, M., I. Petropavlovskikh, R. E. Shetter, S. Hall, K. Ullmann, J. P. Veefkind, R. D. McPeters, E. V. Browell, and P. Levelt, OMI Total Ozone Column Validation with Aura-AVE CAFS Observations, *J. Geophys. Res., 113*(D16), D15S13, doi:10.1029/2007JD008795, 2008a.

Kroon, M., J. P. Veefkind, M. Sneep, R. D. McPeters, P. K. Bhartia, and P. Levelt, Comparing OMI-TOMS and OMI-DOAS total ozone column data, *J. Geophys. Res., 113*(D16), D16S28, doi:10.1029/2007JD008798, 2008b.

Levelt, P. F., et al., Science objectives of the Ozone Monitoring Instrument, *IEEE Trans. Geophys. Remote Sens.,44*(5) 1199-1208, 2006.

Livesey, N. J., M. J. Filipiak, L. Froidevaux, et al., Validation of Aura Microwave Limb Sounder O-3 and CO observations in the upper troposphere and lower stratosphere, *Geophys. Res., 113*(D15), D15S02, 2008.

Logan, J. A., I. Megretskaia, R. Nassar, et al., Effects of the 2006 Elo Niño on tropospheric composition as revealed by data from the Tropospheric Emission Spectrometer (TES), *Geophys. Res. Lett., 35*, L03816, doi:10.1020/2007GL031698, 2008.

Martin, R.V., D.J. Jacob, J.A. Logan, et al., Interpretation of TOMS observations of tropical tropospheric ozone with a global model and in-situ observations, *J. Geophys. Res., 107*(D18), 4351, doi:10.1029/2001JD001480, 2002.

McPeters, R. D., M. Kroon, G. J. Labow, E. Brinksma, D. Balis, I. Petropavlovskikh, J. P. Veefkind, P. K. Bhartia, and P. Levelt, Validation of the Aura Ozone Monitoring Instrument Total Column Ozone Product, *J. Geophys. Res., 113*(D15), D15S14, doi:10.1029/2007JD008802, 2008.

Peters, W., M. Krol, F. Dentener, et al., Identification of an El Nino-Southern Oscillation signal in a multiyear global simulation of tropospheric ozone, *J. Geophys. Res., 106*(D10), 10,398-10,402, 2001.

Schoeberl, M. R., B. N. Duncan, A. Douglass J. Waters, N. Livesey, W. Read, M. Filipiak, The Carbon Monoxide Tape Recorder, *Geophys. Res. Lett.,* 10.1029/2006GL026178, 2006.

Schoeberl, M. R., J. R. Ziemke, B. Bojkov, N. Livesy, B. N. Duncan, et al., A trajectory-based estimate of the tropospheric ozone column using the residual method, *J. Geophys. Res., 112,* D24S49, doi:10.1029/2007JD008773, 2007.

Strahan, S.E., B.N. Duncan and P. Hoor, Observationally-derived diagnostics of transport in the lowermost stratosphere and their application to the GMI chemistry transport model, *Atmos. Chem. Phys., 7,* 2435-2445, 2007.

Sudo, K., and M. Takahashi, Simulation of tropospheric ozone changes during 1997-1998 El Niño: Meteorological impact on tropospheric photochemistry, *Geophys. Res. Lett., 28,* 4091-4094, 2001.

Thompson, A. M., J. C. Witte, R. D. Hudson, et al., Tropical tropospheric ozone and biomass burning, *Science, 291,* 2128-2132, 2001.

Zeng, G., and J. A. Pyle, Influence of El Niño Southern Oscillation on stratosphere/troposphere exchange and the global tropospheric ozone budget, *Geophys. Res., Lett., 32,* L01814, doi:10.1029/2004GL021353, 2005.

Ziemke, J. R., S. Chandra, and P. K. Bhartia, A new NASA data product: Tropospheric and stratospheric column ozone in the tropics derived from TOMS measurements, *Bull. Amer. Meteorol. Soc., 81,* 580-583, 2000.

Ziemke, J. R., S. Chandra, and P. K. Bhartia, A 25-year data record of atmospheric ozone from TOMS Cloud Slicing: Implications for trends in stratospheric and tropospheric ozone, *J. Geophys. Res., 110,* D15105, doi:10.1029/2004JD005687, 2005.

Ziemke, J.R., S. Chandra, B. N. Duncan, L. Froidevaux, P. K. Bhartia, P. F. Levelt, and J. W. Waters, Tropospheric ozone determined from Aura OMI and MLS: Evaluation of measurements and comparison with the Global Modeling Initiative's Chemical Transport Model, *J. Geophys. Res.,* 10.1029/2006JD007089, 2006.

**Table 1:** Emissions of CO and NO for 2006.

| | CO (Tg) | | NO (Tg) | |
|---|---|---|---|---|
| | *Indonesia*[a] | *World*[b] | *Indonesia*[a] | *World*[b] |
| July | 5.9 | 92 | 0.10 | 7.3 |
| August | 16.6 | 103 | 0.29 | 7.4 |
| September | 18.3 | 99 | 0.32 | 6.8 |
| October | 44.2 | 73 | 0.76 | 6.3 |
| November | 6.3 | 79 | 0.11 | 6.3 |
| December | 0.2 | 103 | 0.00 | 7.1 |

[a]Biomass burning emissions only.

[b]Emissions from all sources, including fossil fuels, biofuels, and biomass burning, except biomass burning from Indonesia.

**Table 2.** Monthly Averaged Global Tropospheric Burden of CO, $O_3$, and $NO_X$ for the Model.

| | Sep. | Oct. | Nov. | Dec. |
|---|---|---|---|---|
| | | | CO (Tg) | |
| Indonesia | 351 | 371 | 371 | 369 |
| No Indonesia | 336 | 335 | 329 | 341 |
| ΔCO | 15 | 36 | 42 | 28 |
| ΔCO (%) | 4.6% | 10.7% | 12.6% | 8.1% |
| | | | $O_3$ (Tg) | |
| Indonesia | 354 | 351 | 346 | 332 |
| No Indonesia | 347 | 343 | 337 | 324 |
| $\Delta O_3$ | 8 | 8 | 10 | 8 |
| $\Delta O_3$ (%) | 2.2% | 2.4% | 2.8% | 2.4% |
| | | | $NO_X$ (Tg N) | |
| Indonesia | 0.115 | 0.121 | 0.129 | 0.133 |
| No Indonesia | 0.113 | 0.117 | 0.128 | 0.133 |
| $\Delta NO_X$ | 0.002 | 0.004 | 0.001 | -0.000 |
| $\Delta NO_X$ (%) | 2.1% | 3.0% | 0.8% | -0.3% |

Simulations with ("Indonesia") and without ("No Indonesia") the 2006 Indonesia fire emissions.

**Figure Captions.**

Figure 1. (a) Tropospheric column ozone measured in DU from OMI/MLS for October 2004 (top panel), October 2005 (middle panel), and October 2006 (bottom panel). (b) Same as (a) but instead for the GMI model. (c) The difference (GMI minus OMI/MLS) between Figure 1a and Figure 1b.

Figure 2. (a) Inter-annual difference (October 2006 minus October 2005) of tropospheric column ozone measured in DU from OMI/MLS (top panel) and the GMI model (bottom panel). (b) Same as (a) but instead for November. (c) Same as (a) but instead for December.

Figure 3. (a) Inter-annual annual difference (October 2006 minus October 2005) of 215 hPa CO from MLS (top panel) and 227 hPa CO from the GMI model (bottom panel). All quantities represent volume mixing ratio in units ppbv. (b) Same as (a) but instead for November. (c) Same as (a) but instead for December.

Figure 4. (a) Inter-annual difference (October 2006 minus October 2005) of GMI tropospheric column ozone (in DU) of the Indonesia biomass burning component (top panel) and the dynamically driven component (bottom panel). (b) Same as (a) but instead for November. (c) Same as (a) but instead for December.

Figure 5. OMI/MLS time series ΔTCO (dark curve) plotted with Niño 3.4 time series ΔSST (light curve). ΔTCO is measured in DU while ΔSST is in Celsius degrees and was multiplied by a factor of three for scaling with ΔTCO. The ΔTCO time series is derived by subtracting TCO in the eastern Pacific (15°S-15°N, 135°W-180°) from TCO in the western Pacific (15°S-15°N, 95°E-140°E). The ΔTCO time series was deseasonalized and was also smoothed with a three-month running average to be compatible with the Niño 3.4 time series.

Figure A1. Monthly time series comparisons of GMI (dotted curves) and OMI/MLS (solid curves) tropospheric column $O_3$ (in DU) for three separate regions: American (left four panels), African (middle four panels), and Indonesian (right four panels).

Figure A2. (top) Zonal correlations between OMI/MLS and GMI tropospheric column $O_3$. (middle) Calculated mean zonal offset difference (GMI minus OMI/MLS) measured in DU between model and observation. (bottom) Calculated zonal RMS of difference (GMI minus OMI/MLS) in DU. For both model and observation, fields for similar months (January - December) from 2004 to 2006 where averaged together to derive mean 12-month latitude-longitude gridded distributions of tropospheric $O_3$. All statistical calculations were done zonally for each latitude band using the 72 gridded longitudinal values from model and observation.

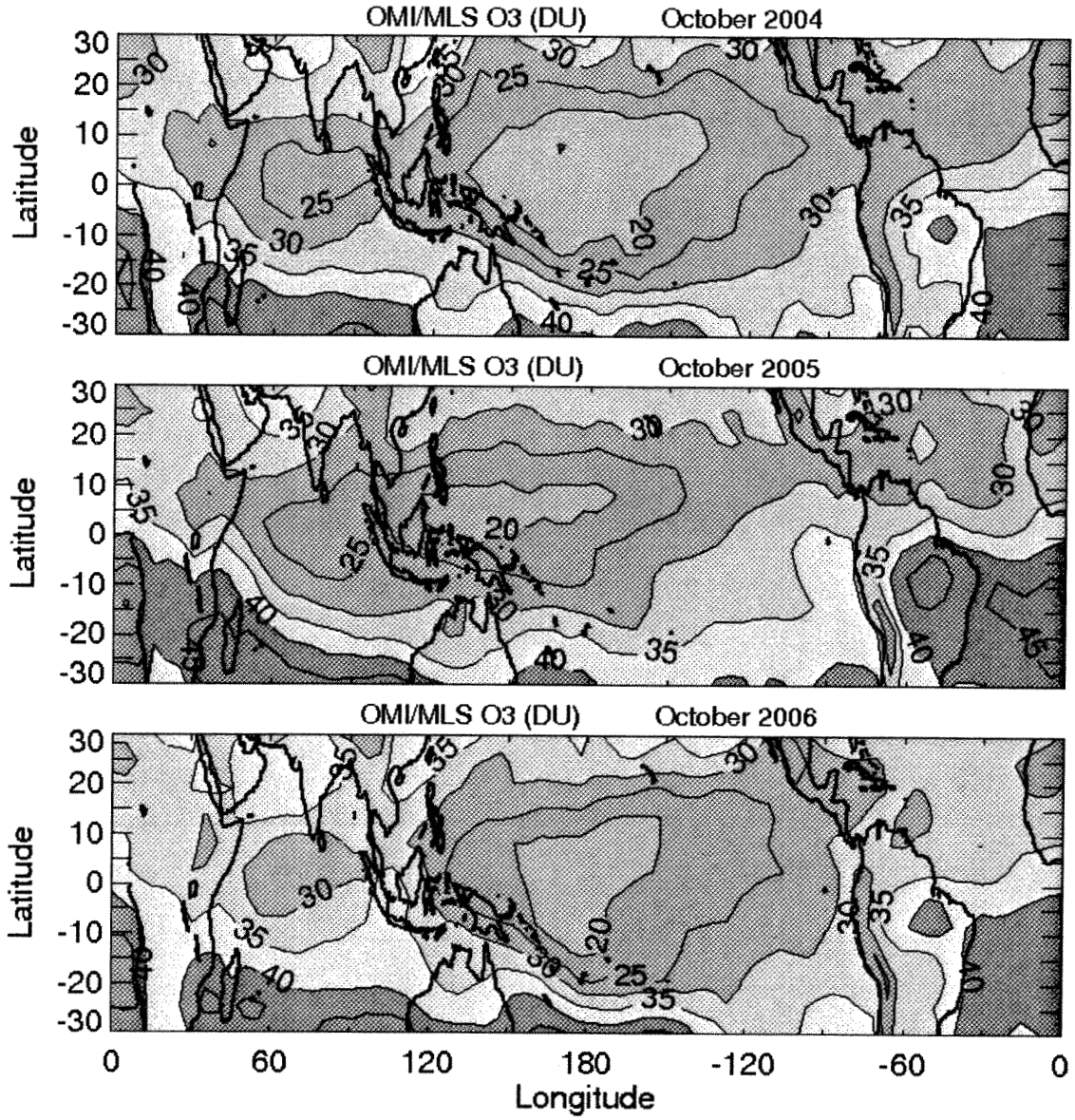
OMI/MLS O3 (DU) October 2004
OMI/MLS O3 (DU) October 2005
OMI/MLS O3 (DU) October 2006
Latitude
Longitude
30
20
10
0
-10
-20
-30
0
60
120
180
-120
-60
0

(Figure 1a)

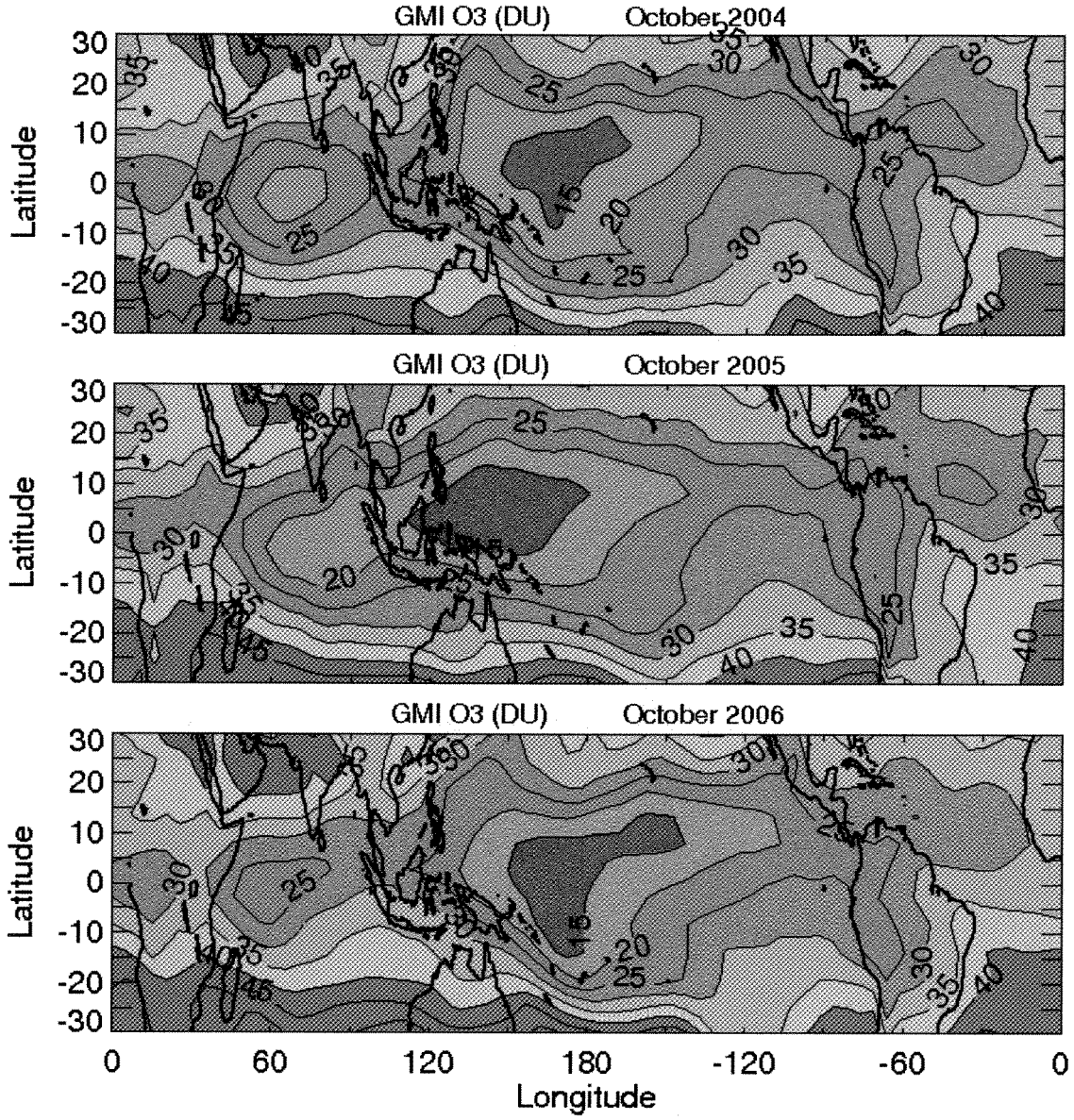
GMI O3 (DU) October 2004
GMI O3 (DU) October 2005
GMI O3 (DU) October 2006
Latitude
Longitude
30
20
10
0
-10
-20
-30
0
60
120
180
-120
-60
0

(Figure 1b)

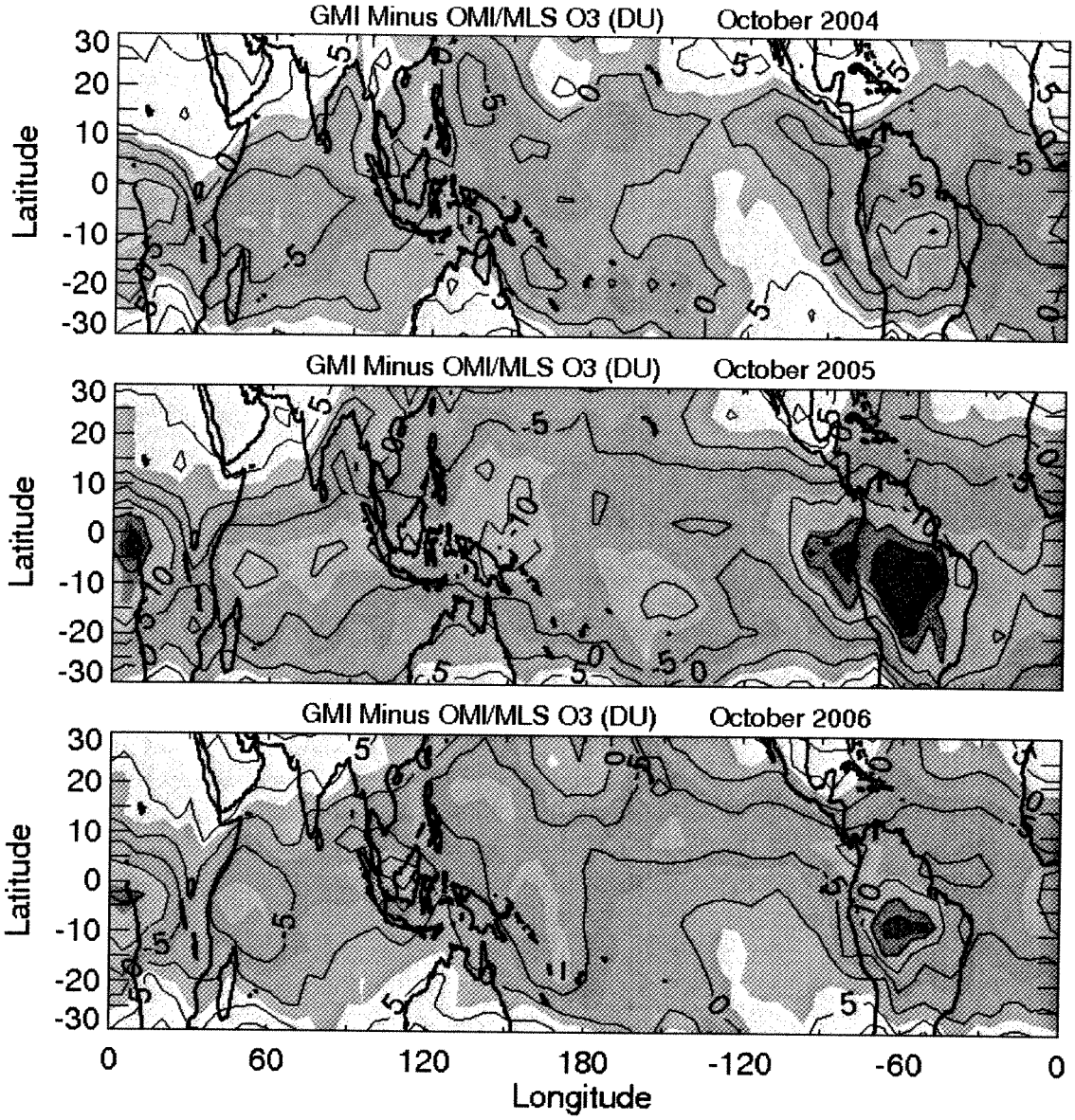
GMI Minus OMI/MLS O3 (DU) October 2004
GMI Minus OMI/MLS O3 (DU) October 2005
GMI Minus OMI/MLS O3 (DU) October 2006
Latitude
Longitude
30
20
10
0
-10
-20
-30
0
60
120
180
-120
-60
0

(Figure 1c)

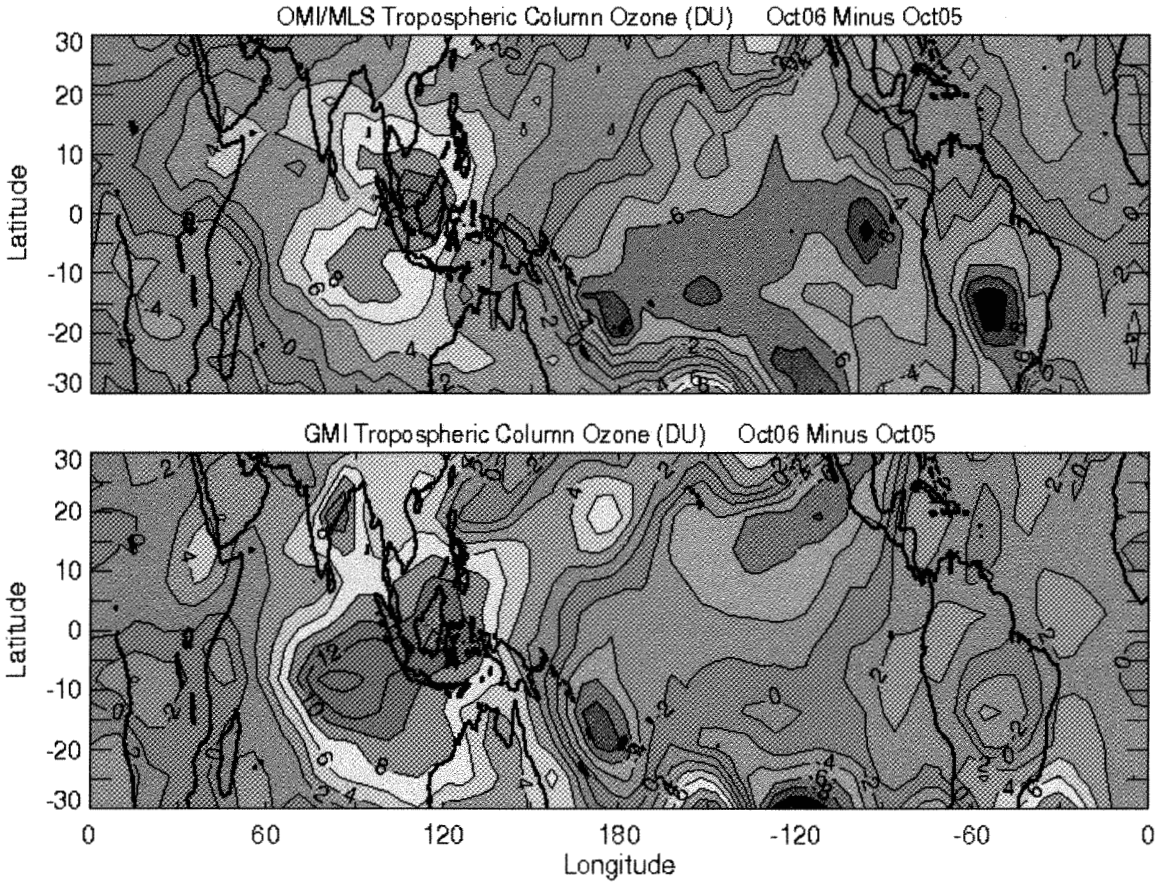
OMI/MLS Tropospheric Column Ozone (DU) Oct06 Minus Oct05
GMI Tropospheric Column Ozone (DU) Oct06 Minus Oct05
Latitude
Longitude
30
20
10
0
-10
-20
-30
0
60
120
180
-120
-60
0

(Figure 2a)

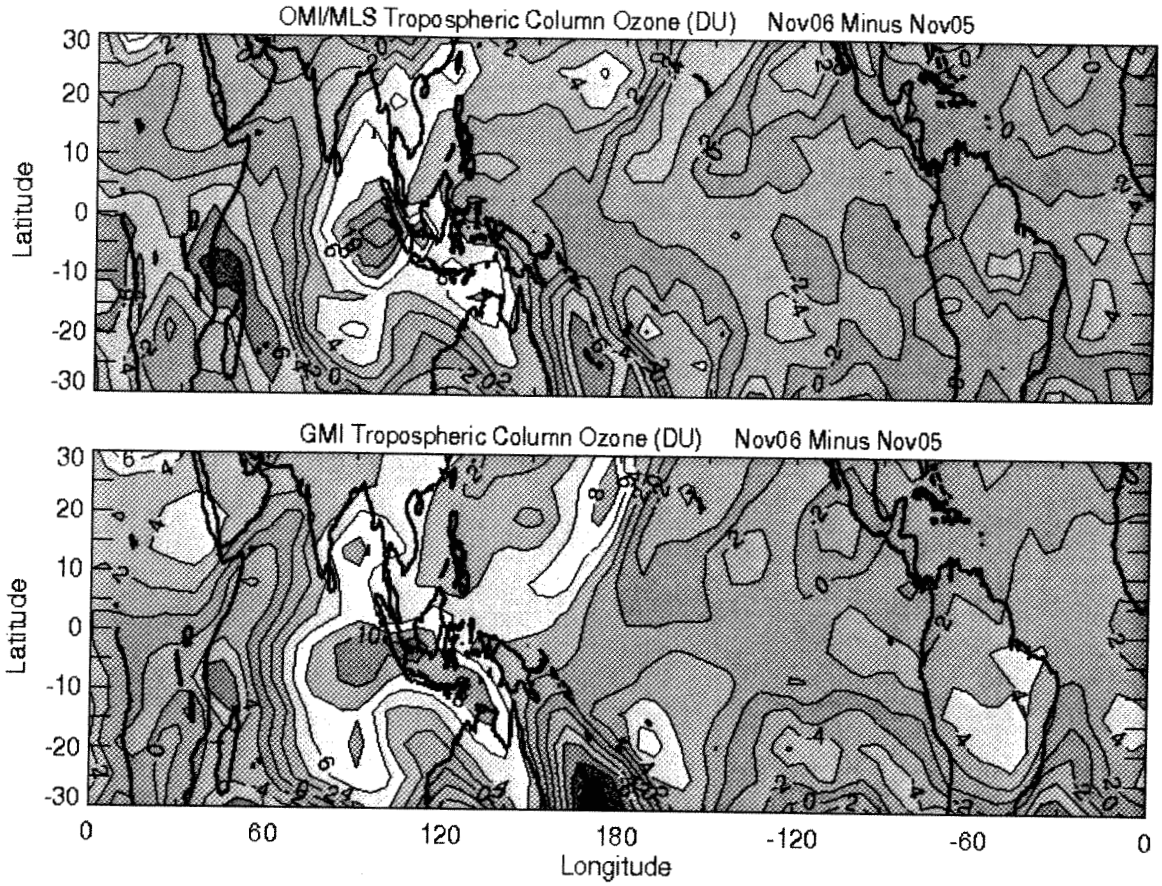
OMI/MLS Tropospheric Column Ozone (DU) Nov06 Minus Nov05
GMI Tropospheric Column Ozone (DU) Nov06 Minus Nov05
Latitude
Longitude
30
20
10
0
-10
-20
-30
0
60
120
180
-120
-60
0

(Figure 2b)

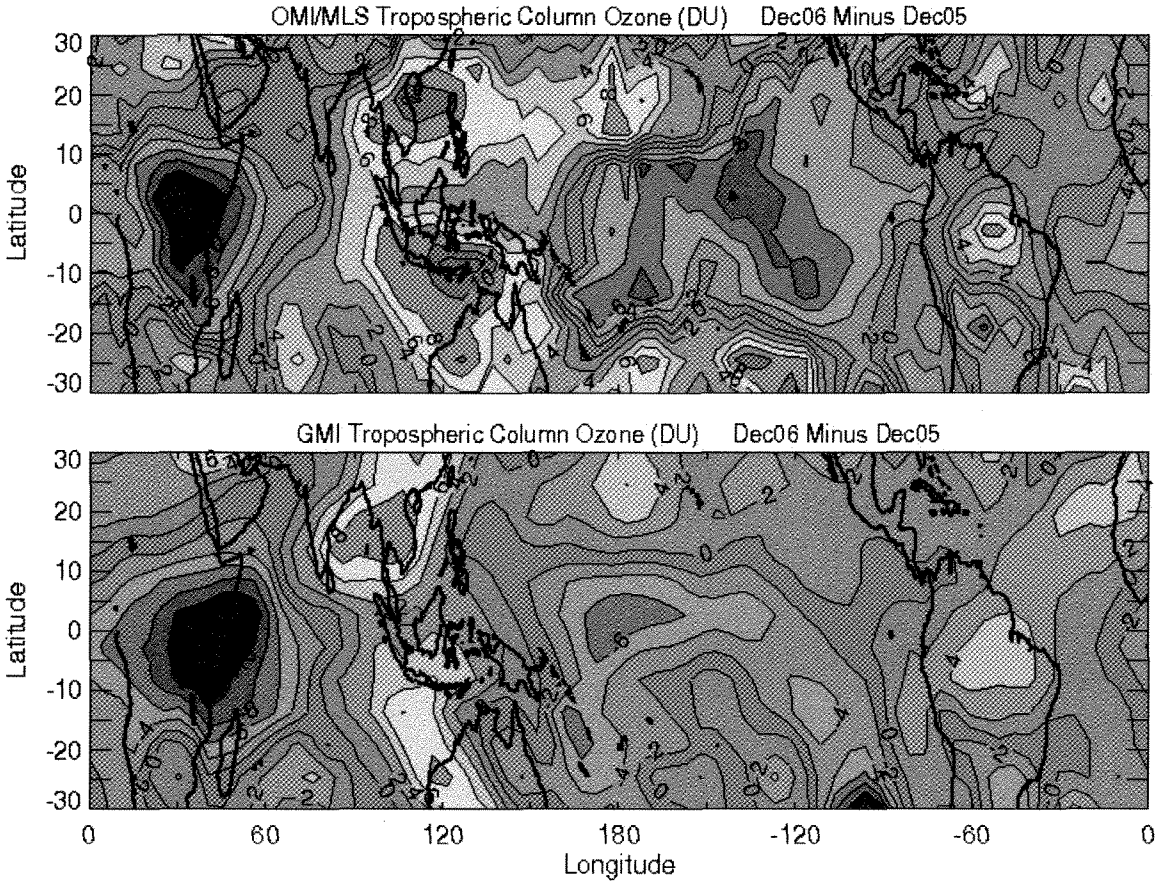
OMI/MLS Tropospheric Column Ozone (DU) Dec06 Minus Dec05
GMI Tropospheric Column Ozone (DU) Dec06 Minus Dec05
Latitude
Longitude
30
20
10
0
-10
-20
-30
0
60
120
180
-120
-60
0

(Figure 2c)

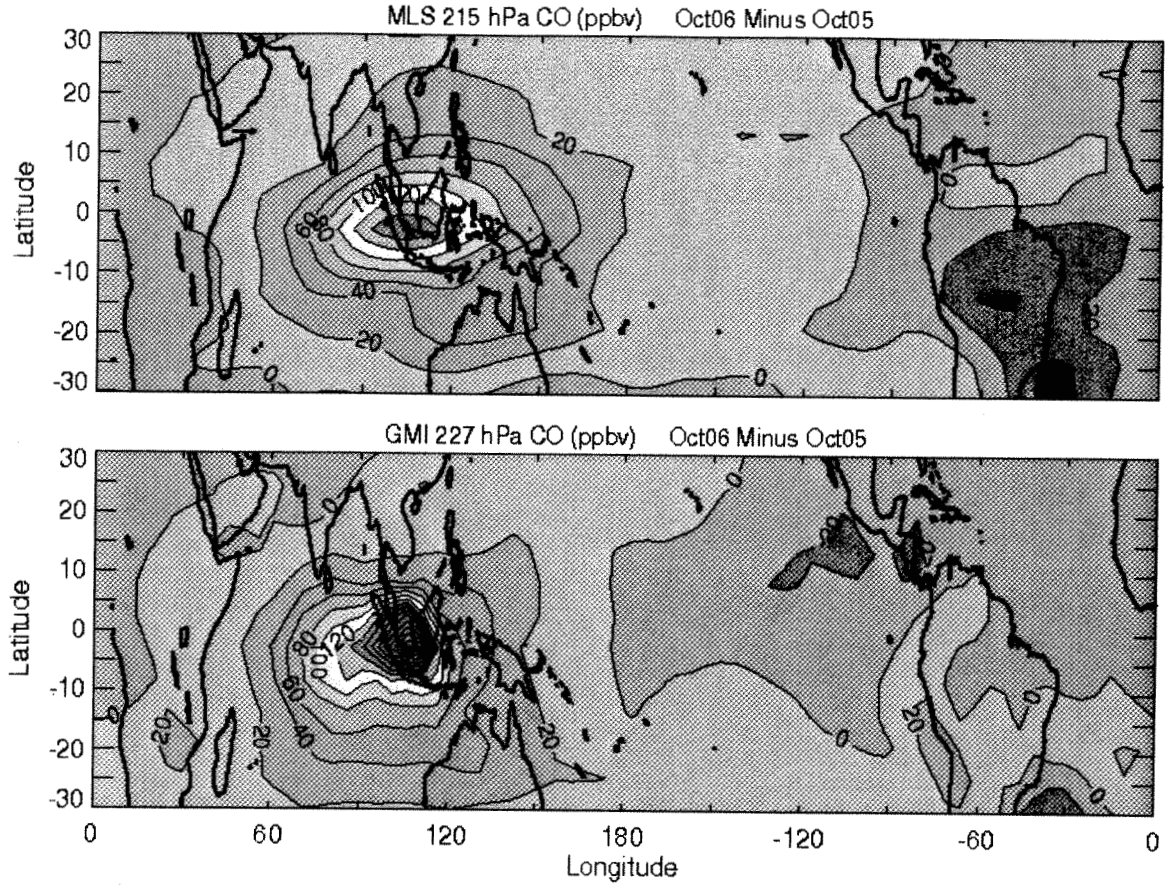
MLS 215 hPa CO (ppbv) Oct06 Minus Oct05
GMI 227 hPa CO (ppbv) Oct06 Minus Oct05
Latitude
Longitude
30
20
10
0
-10
-20
-30
0
60
120
180
-120
-60
0

(Figure 3a)

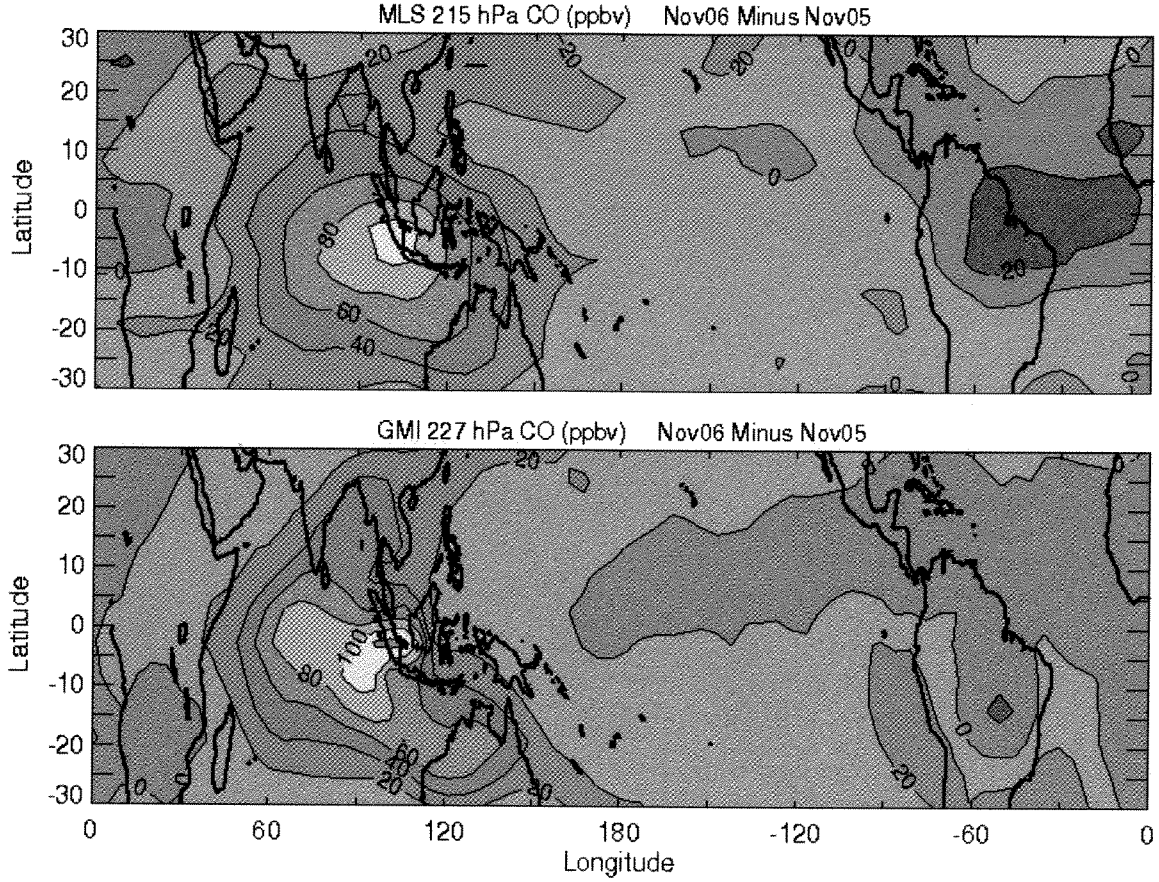
MLS 215 hPa CO (ppbv) Nov06 Minus Nov05
GMI 227 hPa CO (ppbv) Nov06 Minus Nov05
Latitude
Longitude
30
20
10
0
-10
-20
-30
0
60
120
180
-120
-60
0

(Figure 3b)

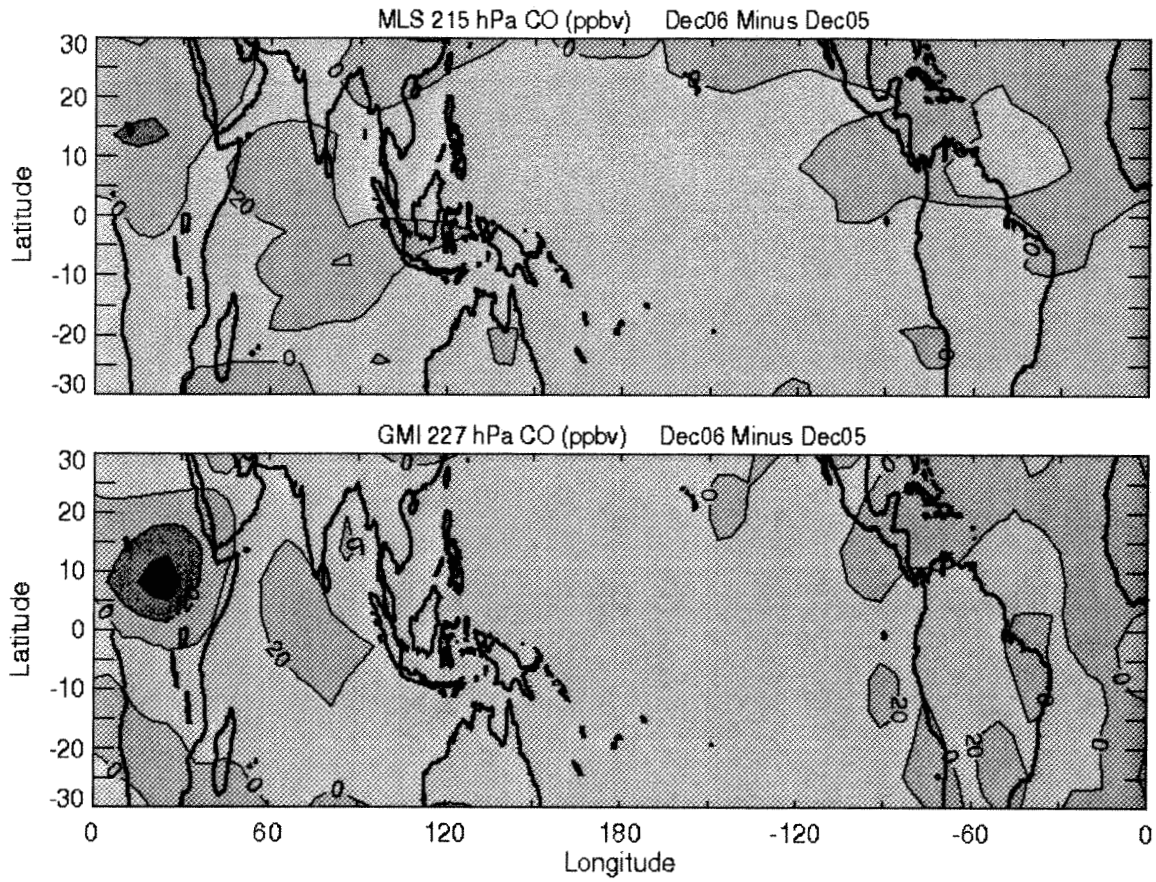
MLS 215 hPa CO (ppbv) Dec06 Minus Dec05
GMI 227 hPa CO (ppbv) Dec06 Minus Dec05
Latitude
Longitude
30
20
10
0
-10
-20
-30
0
60
120
180
-120
-60
0

(Figure 3c)

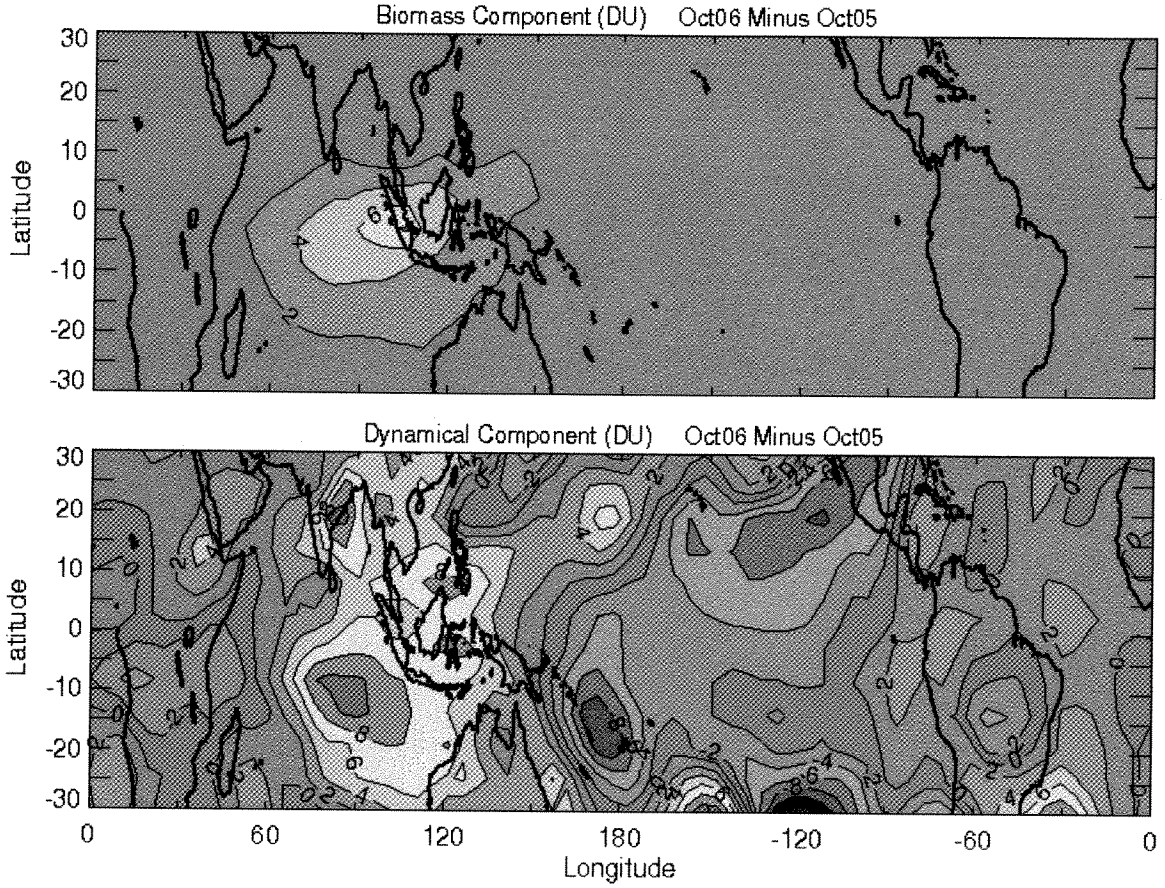
Biomass Component (DU) Oct06 Minus Oct05
Dynamical Component (DU) Oct06 Minus Oct05
Latitude
Longitude
30
20
10
0
-10
-20
-30
0
60
120
180
-120
-60
0

(Figure 4a)

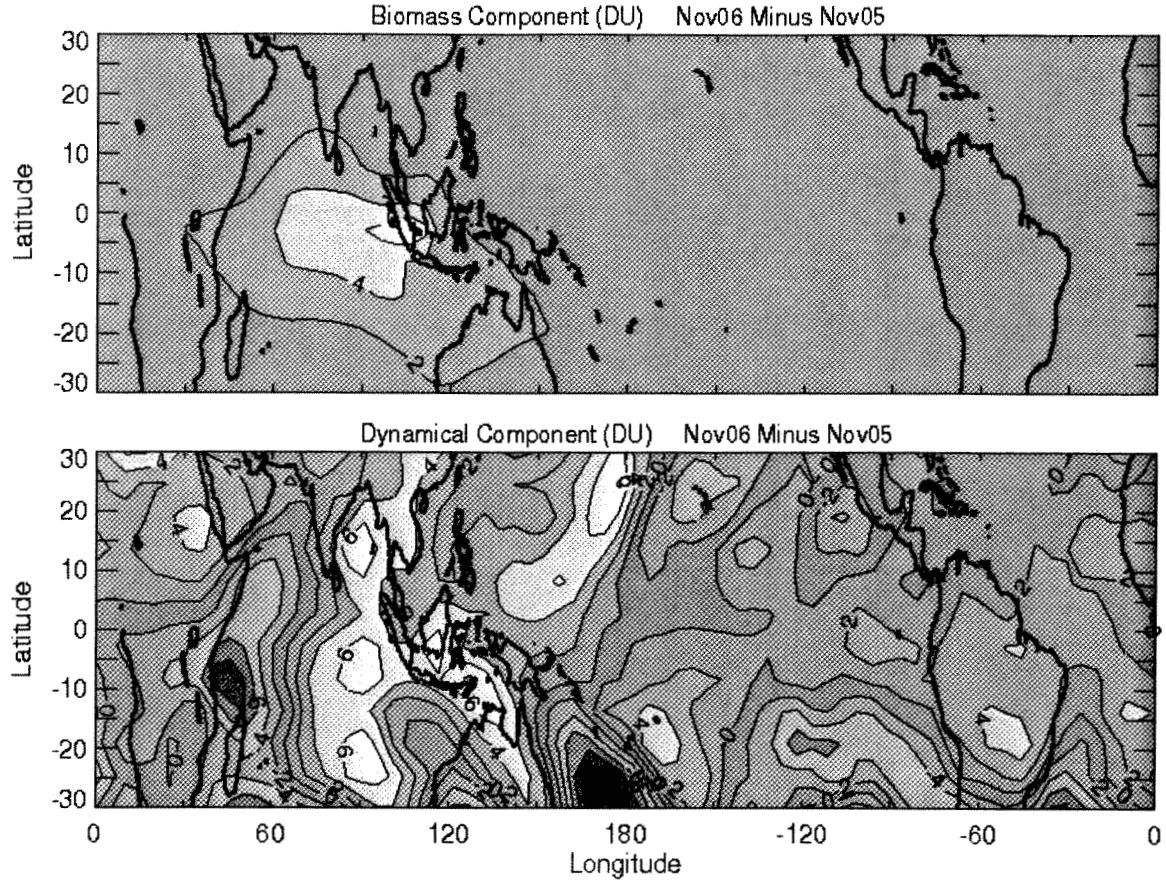


(Figure 4b)

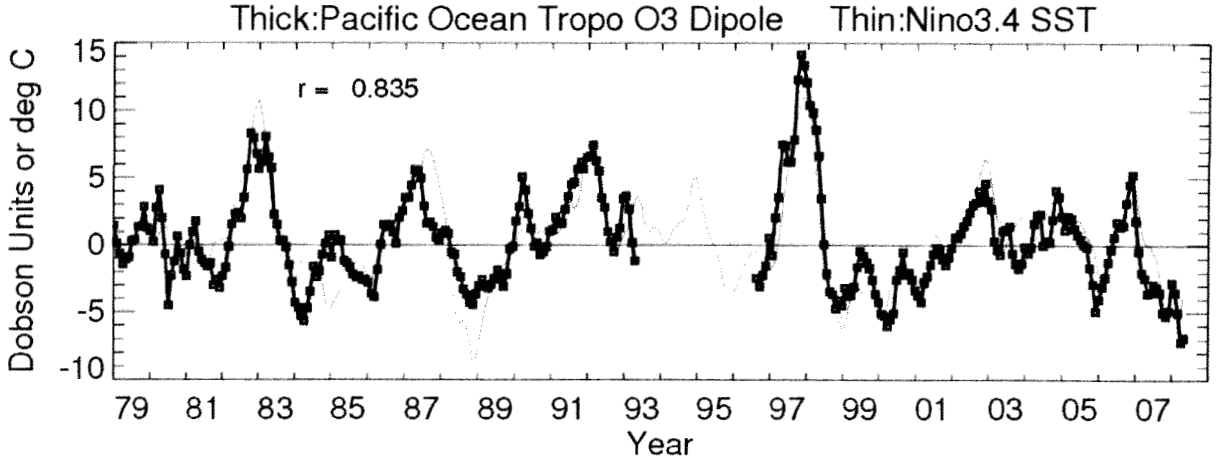


(Figure 5)

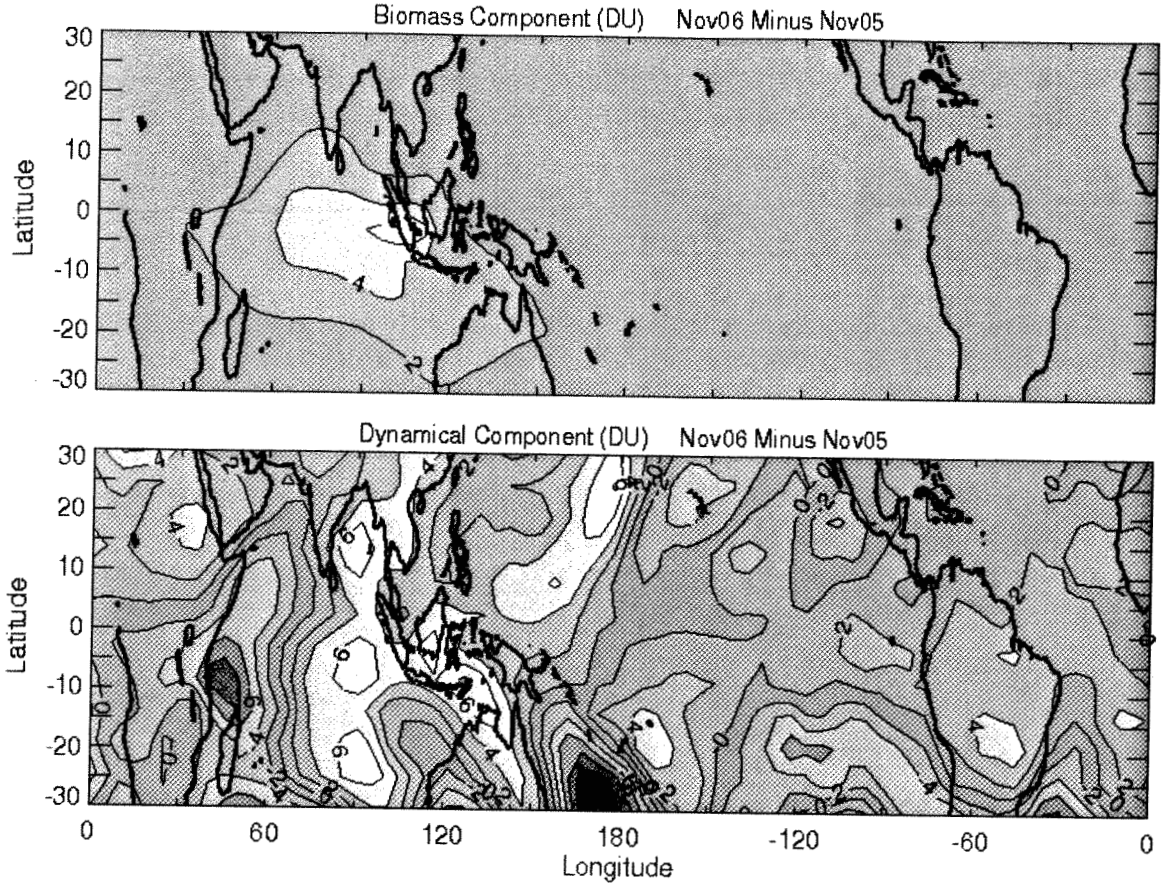


(Figure 4b)

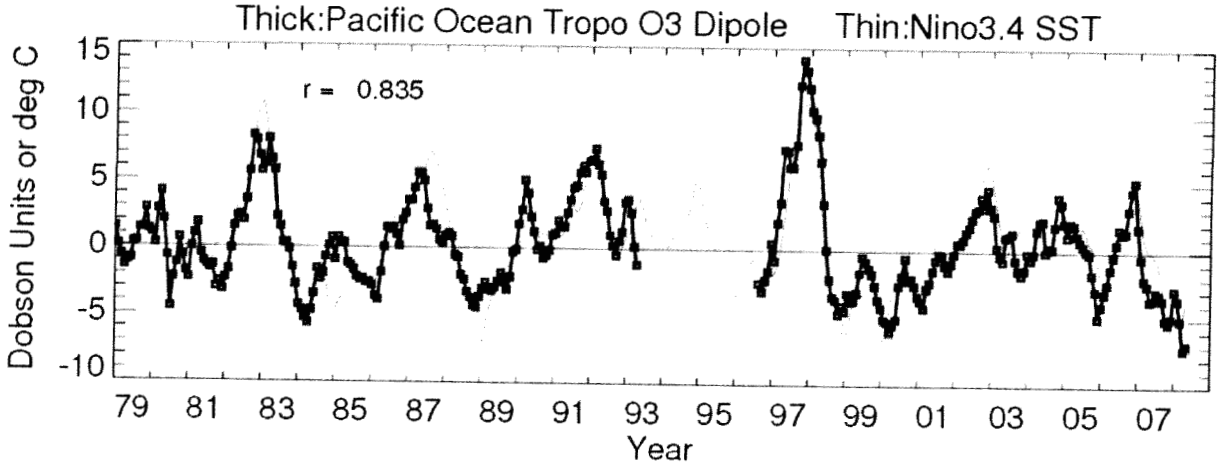


(Figure 5)

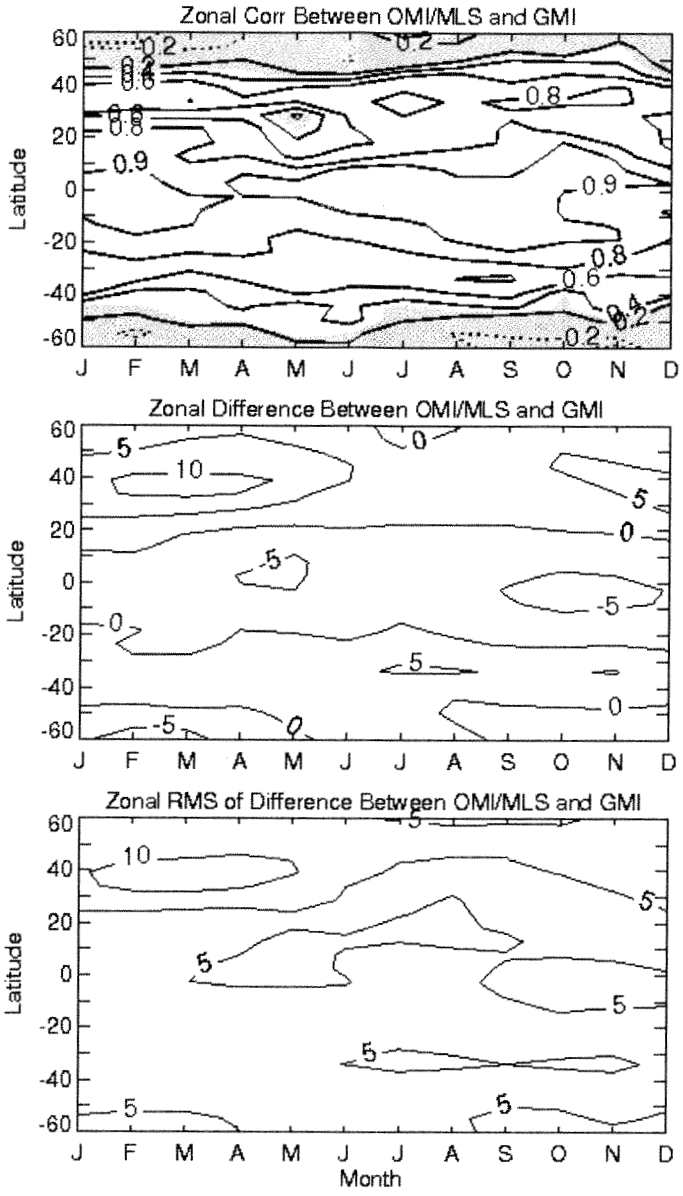
Zonal Corr Between OMI/MLS and GMI
Zonal Difference Between OMI/MLS and GMI
Zonal RMS of Difference Between OMI/MLS and GMI
Latitude
Month
J F M A M J J A S O N D
60
40
20
0
-20
-40
-60

(Figure A2)